RSC Advances

PAPER

Cite this: *RSC Adv.*, 2021, **11**, 33093

Scaling law for the kinetics of water imbibition in polydisperse foams

Kanoko Tsuritani[a] and Susumu Inasawa *[abc]

We investigated the kinetics of water imbibition in polydisperse foams. We used a Hele-Shaw cell, and horizontal imbibition was observed for a timescale of up to 10^3 s in which the gravity effect was negligible. While several papers have reported kinetics for imbibition in foams, imbibition kinetics in polydisperse foams and its variations in longer timescales are not well understood. The tip position of imbibition was proportional to the square root of time in the initial stage of imbibition, but it showed plateauing in the late stage of imbibition. We evaluated the proportional constant A in the initial stage of imbibition as a kinetic constant for the time-dependent increase in the tip position, which showed a clear dependency on the initial and final water volume fractions in the foams. Conversely, the mean initial radius of the curvature and the channel length in the Plateau borders did not show any clear correlations with A, although both valuables are frequently used in modeling for liquid imbibition in foams. On the basis of the $t^{1/2}$ dependence, the correlation of A with the water volume fraction and the increase in the water volume fraction during imbibition, we proposed a simple equation to describe the tip position over the entire period of imbibition. We used them to scale all of the experimental data, which showed good agreement with the theoretical line. This clearly showed that the water volume fraction in the foams during imbibition was the key factor to quantitatively describe the rate of water imbibition. Features in the kinetics of imbibition were discussed.

Received 24th August 2021
Accepted 26th September 2021

DOI: 10.1039/d1ra06392h

rsc.li/rsc-advances

1. Introduction

Foam is an ensemble of bubbles separated by thin liquid layers. The gas–liquid interfaces are generally deformable, which provides a complicated structure of a connected network of thin liquid layers. Gas molecules permeate through liquid films,[1] and coarsening,[1,2] rearrangement,[3] and destabilization[4] of the bubbles frequently occur in foams. The surface elasticity of bubbles is an important factor for coarsening and coalescence[5] because of the large gas–liquid interfacial area in foams. Osmotic pressure emerges in foams depending on the liquid volume fraction, size of the bubbles, and gas–liquid interfacial energy.[6,7] To understand the complicated properties of foams, theoretical approaches have also been used to describe deformation of the bubbles[8] and the response to shear fields.[9] These are only a few examples, but they clearly show the unique properties of foams originating from the gas–liquid interfaces.

Many thin liquid channels are connected in foams, and the flow in these channels is an intensely studied topic. A narrow channel of liquid typically surrounded by three contacting bubbles is called Plateau border and many Plateau borders are connected by junctions called nodes. These connected paths are the main routes for liquid flow in foams. Cutting-edge approaches have been developed to measure the flow in a single Plateau border formed by a triangular prism frame[10–12] or three-dimensional (3D) printing.[13] The distribution of flow velocities in an exterior or interior channel of the Plateau border has been measured by particle tracking.[14] The mobility and surface viscosity on the gas–liquid interfaces are the main factors that affect the flow velocity in Plateau borders,[14,15] whereas it has been reported that there is no close relation between the interfacial shear elasticity and liquid entrainment on foam films.[16] Studies on the spontaneous flow of liquid in a narrow gap between rods[17] or bubbles[18] has also provided useful information about the liquid flow in a Plateau border between packed bubbles. The flow in nodes and its differences from the flow in channels have been experimentally investigated.[19,20] The cross section of the Plateau border and the channel length have been mathematically modeled using a geometric relation,[21,22] with which conservation of the liquid volume during flow is considered.[23–26] Both the experimental and theoretical work on the microscopic flow in foams are summarized in ref. 27. Similar Plateau borders form in

[a]*Graduate School of Bio-Applications and Systems Engineering, Tokyo University of Agriculture and Technology, 2-24-16 Nakacho, Koganei, Tokyo 184-8588, Japan. E-mail: inasawa@cc.tuat.ac.jp*

[b]*Department of Applied Physics and Chemical Engineering, School of Engineering, Tokyo University of Agriculture and Technology, 2-24-16 Nakacho, Koganei, Tokyo 184-8588, Japan*

[c]*Department of Chemical Engineering, School of Engineering, Tokyo University of Agriculture and Technology, 2-24-16 Nakacho, Koganei, Tokyo 184-8588, Japan*

concentrated emulsions,[28–31] and these models for the flow between bubbles are used to simulate the pressure distribution in packed droplets in drying emulsions.[28,29]

The flow of liquid through many Plateau borders and nodes is measurable experimentally using foam drainage or imbibition of the liquid into dry foam. In foam drainage, the liquid phase drains owing to gravity, which has been extensively investigated experimentally and theoretically.[32–38] The moving rate of the wetting front is proportional to the square root of the rate of liquid addition to a monodisperse foam.[32] The mobility parameter M, which incorporates bubble size, liquid content and surface shear viscosity of bubbles has been proposed as a relevant parameter to describe foam drainage regimes.[36] In the case of emulsions or colloidal suspensions, dispersed oil droplets or solid particles are trapped in the water paths in the foams, which reduces the rate of drainage compared to that without droplets or solid particles.[39–41]

Imbibition of liquid into a foam occurs owing to the capillary pressure of the Plateau border, and comparison with the gravity effect is the key to imbibition on earth.[42,43] Microgravity has been investigated in liquid imbibition to minimize the effect of gravity,[44–50] in which the bubbles are very stable and coarsening or coalescence does not occur.[50] Imbibition can be explained by a diffusion-like process and the wetting front is proportional to the square root of time.[46] In the case of dry foam under microgravity, the proportional constant of $A = 1.19\ \mathrm{cm^2\ s^{-1}}$, is reported,[46] but this value would vary depending on foams. The diffusion-like process of the wetting front has been supported by modeling and the corresponding diffusion equations have been theoretically derived.[44,46,48,51] Prediction of the A value from experimental data has also been performed.[46,51] However, one important point is that most reported microgravity experiments were mainly conducted in a falling plane and the experimental time for imbibition was inevitably limited (up to at most 20 s).[45,46,48] We do not understand how imbibition proceeds for longer time scales. In addition, a number of reported A values are rather limited[46,48] and the generality of this approach to other polydisperse foams and the range of A are still unknown. Our motivation for this work is to clarify these points. Imbibition is a fundamental phenomenon in foams and it consists of the microscopic flows in many Plateau borders. Thus, this study is important to understand the features of liquid flow in foams.

In this study, we observed water imbibition in aqueous foams. For visual observation, the foam was introduced into the gap between two parallel glass plates (Hele-Shaw cell). To avoid the gravity effect, we set the samples horizontally and forced dyed aqueous solution to contact the foam. We used polydisperse foams with various initial water fractions. The change of the position of the imbibition front with time was measured. The correlations between the rate constant for imbibition and the relevant parameters of foams are also discussed.

2. Experimental methods

Sodium dodecyl sulfate (SDS) (Fujifilm Wako Pure Chemical Co., Osaka, Japan) and polyoxyethylene(10) octylphenyl ether (TX-100) (Fujifilm Wako Pure Chemical) were used as surfactants. We prepared aqueous surfactant solutions containing 8 mM SDS and 1 mM TX-100. The interfacial energies (surface tensions) of these solutions were 42 mN $\mathrm{m^{-1}}$ for SDS and 33 mN $\mathrm{m^{-1}}$ for TX-100, both of which were determined by the capillary rise method (DG-1, Surfgage Instruments, Matsudo, Chiba, Japan). We also prepared surfactant solutions with the same concentrations but dyed with uranine (Fujifilm Wako Pure Chemical). We used the dyed solutions for imbibition observation.

Air was introduced into the solutions through a glass tube with an inner diameter of 5 mm. The tip of the tube was fully covered by a filter paper (Munktell M1-125, Ahlstrom Corporation, Helsinki, Finland). We changed the air flow rate in the range 50–200 mL $\mathrm{min^{-1}}$ to vary the sizes of the bubbles and their distribution. After the bubbling, the bubbles were spontaneously accumulated on the top of the solutions and we obtained foams. The solutions were left to stand for various periods to change the liquid-volume fraction in the foam. We placed a specified amount of the foam in an observation cell, which is schematically illustrated in Fig. 1 (bottom). We fabricated the observation cells using a set of slide glasses and spacers. Two spacers with a height of 0.5 mm was set on the slide glass in parallel. The width between the spacers was 35 mm. We placed aqueous foam between the spacers and set the other slide glass on them so that the foam was sandwiched between the slide glasses. The total length of the foam between the glasses was approximately 5–6 cm. We then placed an amount of the dyed surfactant solution on one side of the cell. Spontaneous imbibition of the dyed surfactant solution was observed and recorded by an optical microscope (AZ-100, Nikon, Tokyo, Japan) equipped with a digital camera (D-5200, Nikon). We used an objective lens (AZ-Plan Apo 0.5×, Nikon). An example of imbibition observation is shown in Fig. 1 (top). The time intervals for recording were 3 s for the initial fast imbibition and 20 s for the later slow imbibition. Bubbles were flexible and shape change in bubbles spontaneously occurred owing to water imbibition within the time intervals of 3 s. We observed water imbibition in a timescale of up to 10^3 s.

The recorded images were analyzed using the free software ImageJ (National Institute of Health, USA). We measured the

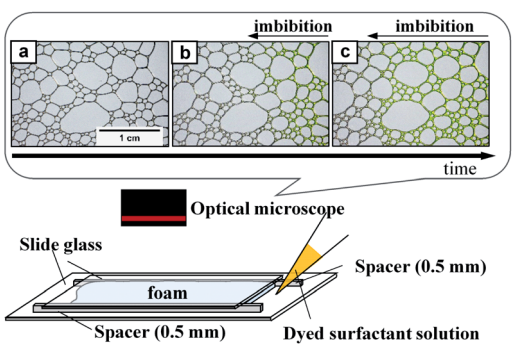

Fig. 1 (Top) Optical microscope images of imbibition. The dyed surfactant solution imbibed from right to left, as shown in (a)–(c). (Bottom) Schematic illustration of the experimental setup used in this study.

imbibition length of the foam, from the injection edge of the cell to the tip of the imbibition as defined in Fig. 1b and c. In addition, we measured the radius of curvature and channel length of the bubbles in the foam. Definitions of these valuables are shown in Fig. 3. We also estimated the total air area of the bubbles using the commercial software MATLAB (Mathworks Inc., Natick, MA, USA), with which we estimated the water volume fraction in the foam.

The numerical aperture of the objective lens was 0.05 and the resolution limit of the lens was estimated to be 6 μm. We also checked the resolution of the recorded digital images, which was 10 μm per pixel. The minimum length scale discussed in this work is 0.1 mm and we confirmed that the observed images had sufficient resolution.

In estimation of the water volume fraction, we first estimated the total area of the bubbles surrounded by gas–liquid interfaces. We then subtracted it from the total area of the foam. Owing to the curved shape of the interfaces, they were recorded as black lines with a width in the images. In our analysis, these lines were counted as the water phase, but both air and water were present in these black line regions owing to the curved interfaces. This suggests that the estimated water volume fraction would overestimate the actual value. However, we did not aim to determine the precise value of the water fraction, and hence we used the estimated water fraction in this work. The estimated values of the initial water volume fraction before imbibition were in the range 0.18–0.59 and those of the final water volume fraction after the end of imbibition were in the range 0.40–0.70.

3. Results

Optical microscope images of the foams before imbibition are shown in Fig. 2a–c. The corresponding distributions of the radius of curvature r_{curv}, circular radius r_{circle}, channel length of the Plateau border L_{nn} are shown in Fig. 3. The definition of r_{circle} is shown in Fig. 3b. The bubbles in the foams we used were

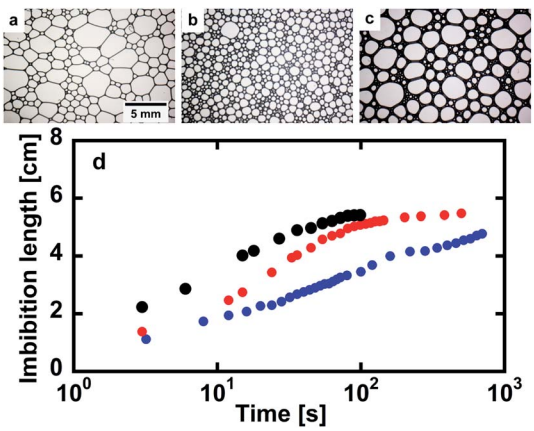

Fig. 2 (a)–(c) Optical microscope images of three different foams. (d) Changes of the imbibition lengths with time. The data for the foams in (a), (b) and (c) are represented by black, red, and blue symbols in (d), respectively.

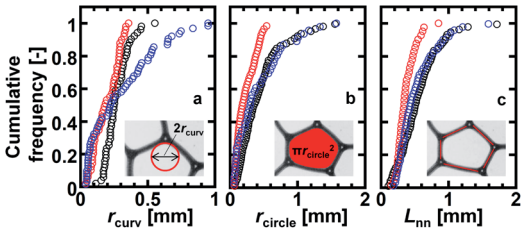

Fig. 3 Cumulative frequencies of the initial values of the (a) radius of curvature (r_{curv}), (b) circular radius (r_{circle}), and (c) channel length of the Plateau border (L_{nn}) for the three different foams. The black, red, and blue symbols are for the foams in Fig. 2(a–c), respectively. The definitions of r_{curv}, r_{circle}, and L_{nn} are schematically shown in the inserts.

polydisperse and they had different distributions of these characteristic values (Fig. 3). The change of the imbibition length with time is shown in Fig. 2d. Imbibition of water varied depending on the foam, and the rate of imbibition decreased with time. Images of the bubbles at three different positions during imbibition are shown in Fig. 4. Before imbibition, the bubbles were packed and distorted at all positions (images 1–3 in Fig. 4a). After 30 s imbibition (Fig. 4b), the bubbles near the

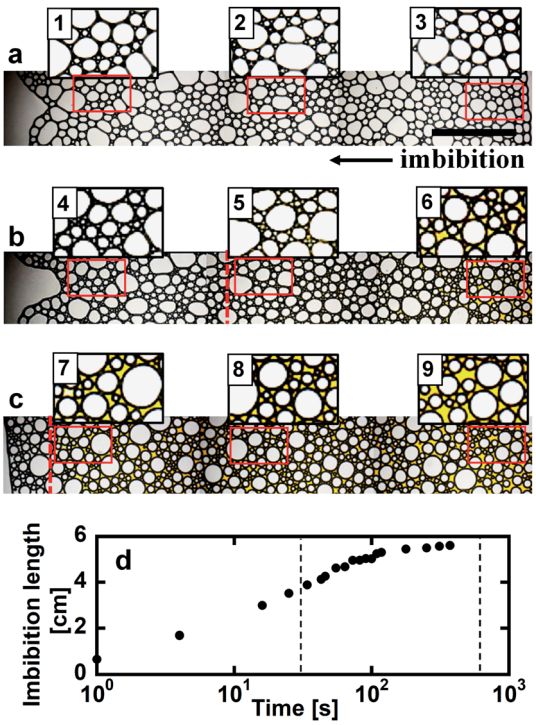

Fig. 4 Optical microscope images of a foam in different imbibition states: (a) before imbibition and (b) 30 s and (c) 600 s after the beginning of imbibition. Imbibition proceeded from right to left. The entire foam was horizontally long and we recorded the foam at three different positions and overlaid them to obtain the long horizontal images of (a)–(c). Images 1–9 are enlarged images of the parts of the foam indicated by the red boxes in (a)–(c). The vertical red dashed lines in (b) and (c) show the tip position of water imbibition. (d) Corresponding change of the imbibition length with time. The dashed lines indicate 30 s and 600 s on the time axis. The scale bar in (a) is 1 cm.

starting point of water imbibition were circular in shape (image 6), while those at different positions near the imbibition tip (image 5) and away from the tip (image 4) were still distorted. In the late stage of imbibition, the tip of imbibition reached the other side of the foam (Fig. 4c), and all of the bubbles became spherical in shape (images 7–9). The correlations between the imbibition length and estimated water volume fraction ε_{water} at three different positions are shown in Fig. 5. We need to define a sufficiently larger area than the bubble sizes to estimate ε_{water}. The sizes of most of the bubbles were less than 1 mm (Fig. 2 and 3). Thus, we used a 13 mm square to estimate the water volume fraction (see the top image of Fig. 5). ε_{water} increased with time for all three areas, but the increase was slower for areas b and c. This suggests that ε_{water} was not uniform in the foams during imbibition. In the late stage of imbibition indicated by the arrows in Fig. 5d and e, there was almost no change in ε_{water} for all areas and ε_{water} was almost constant at around 0.7 (Fig. 5e).

4. Discussion

4.1 Kinetic constant for the initial stage of imbibition

Foam drainage theory is a candidate to describe the change of the tip position of water imbibition.[33,34,36,38] However, this is not practical for this study because the partial differential nature of the fundamental equation in foam drainage theory.[33,34,44,46] Conservation of the volume of the flowing liquid in foams frequently requires both temporal and spatial differential

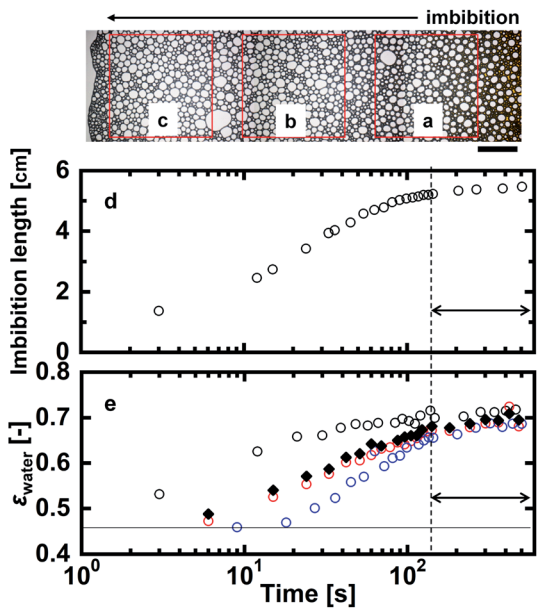

Fig. 5 (Top) Optical microscope image of the foam during imbibition. We estimated the water volume fraction ε_{water} in the three areas indicated by the red squares of (a), (b), and (c) during imbibition. Changes of the (d) imbibition length and (e) ε_{water} with time. The black, red, and blue open circles show ε_{water} in areas (a), (b), and (c) in the top image, respectively. The solid black diamonds in (e) show the average values of ε_{water} over the three areas (a)–(c). The double-headed arrows in (d) and (e) show the periods of the late stage of imbibition. The scale bar in the top image is 5 mm.

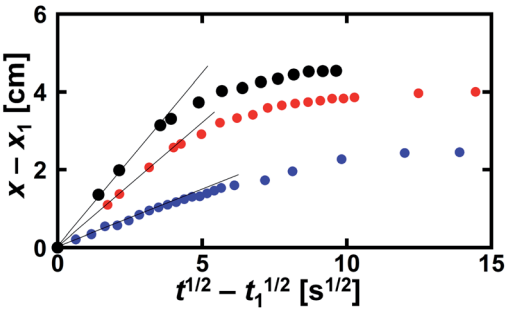

Fig. 6 Data in Fig. 2 replotted using eqn (1). The definitions of the black, red, and blue solid circles are the same as in Fig. 2. The solid lines show the initial slopes of A for the separate data.

formulas. Consequently, the governing equations need to be numerically treated to obtain solutions,[33,34,44,46] which brings complexity into the analysis. Thus, we analyzed the experimental data using a square-root expression.[45,46,48]

Assuming that the tip position of water imbibition $x(t)$ is described by the square root of time, we set $x(t) = At^{1/2}$, where A is a kinetic constant in units of cm s$^{-1/2}$. In several papers, the constant A is called the diffusivity.[45,46] However, as we have already discussed, the origin of water imbibition is flow. Therefore, hereafter, we call A the kinetic constant in this paper. We define $t = 0$ as the time when we added the dyed solution to the observation cell. However, there was a slight delay before the first image of imbibition was recorded. To minimize this experimental error in time, we used the difference in the imbibition length

$$x(t) - x(t_1) = A\left(\sqrt{t} - \sqrt{t_1}\right) \quad (1)$$

where t_1 is the time at which the first image was recorded. We analyzed the data in Fig. 2 using this equation and the results are shown in Fig. 6. All of the data showed a linear increase in the initial stage of imbibition, but the slope decreased with time, which will be discussed in the following section.

Water imbibition occurs because of the negative pressure in the Plateau borders in the foam, which is approximately expressed as γ/r_{curv}, with γ being the interfacial energy on the air–liquid interface. Thus, it is a reasonable interpretation that r_{curv} has a close relation with A. However, there was no clear relation between A and the mean values of the initial r_{curv} (Fig. 7 left). We also plotted A against the mean channel length before

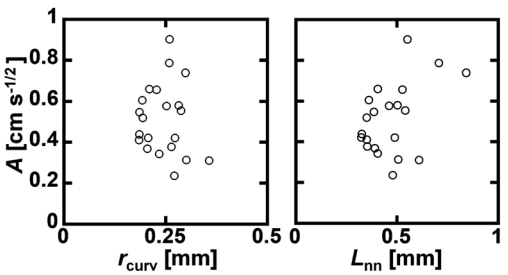

Fig. 7 Correlation between A and the mean initial r_{curv} (left) and mean channel length before imbibition L_{nn} (right).

imbibition L_{nn}, but there was also no close relation with A (Fig. 7 right). Thus, we did not find any clear relation between the initial geometric parameters of the foams and the kinetic constant A. There were wide distributions of r_{curv} and L_{nn} (Fig. 3). This would be a reason why A and r_{curv} did not show a clear correlation (Fig. 7 left). We also measured the cumulative frequencies of the bubble area in the foams during water imbibition, but we did not find any clear change in the distributions during water imbibition.

We found that ε_{water} in the foam increased as imbibition progressed (Fig. 5). It became constant after the rate of increase in the imbibition length was small. In this late stage of imbibition, all of the bubbles were circular in shape (Fig. 4c), suggesting that the foam was saturated with water. We consider that the constant ε_{water} in the late stage of imbibition was the upper limit of ε_{water} in the foam. Water imbibition is a process in which ε_{water} increases in foams. The difference between the final water volume fraction ε_{water_f} and initial volume fraction ε_{water_0} in the same foam corresponds to the amount of water that can be absorbed by the foam. The ratio of the absorbable amount of water to the maximum water volume in a foam $(\varepsilon_{water\_f} - \varepsilon_{water\_0})/\varepsilon_{water\_f}$ would then be correlated with the kinetics of imbibition. Thus, we plotted the A values using $(1 - \varepsilon_{water\_0}/\varepsilon_{water\_f})$ for all of the examined foams (Fig. 8). The samples of SDS and TX-100 both showed good correlations. We concluded that the initial and final volume fractions of water are the key factors to describe water imbibition.

We used a power law formula to describe the dependency of A on $(1 - \varepsilon_{water\_0}/\varepsilon_{water\_f})$. The SDS data agreed well with $A = (1 - \varepsilon_{water\_0}/\varepsilon_{water\_f})^{0.6}$, while $A = 0.89(1 - \varepsilon_{water\_0}/\varepsilon_{water\_f})^{0.6}$ gave the best fitting result for the TX-100 data. This suggests that the rate of water imbibition in the TX-100 foams was about 90% of that in the SDS foams. The surface tension on the air–water interface was 42 mN m^{-1} for SDS and 33 mN m^{-1} for TX-100. The air–water interfacial energy of the TX-100 samples was about 80% of that of the SDS samples, showing reasonable agreement with the proportional constant of 0.89. This simple comparison suggests that the air–water interfacial energy affects A. Thus A would vary depending on types of surfactants and types of gases in foams.

In this study, the kinetic coefficient A varied from 0.2 to 1 cm s$^{-1/2}$ (Fig. 8). In a microgravity experiment, the corresponding coefficient has been reported to be 1.19 cm^2 s^{-1} (1.09 cm s$^{-1/2}$) in a Hele-Shaw cell.[45,46] Our values were smaller but in reasonable agreement with the previous studies. Cox *et al.*[51] predicted this constant as $A^2 = \gamma LK\delta/\eta$, in which L is a relevant length scale for the Plateau border, K is the permeability constant, δ is a geometric constant, and η is the viscosity of the surfactant solution. In this study, L was typically 0.5 mm (Fig. 7 right) and the other values were $\gamma = 42$ mN m^{-1}, $\delta = 0.655$,[51] and $\eta = 1 \times 10^{-3}$ Pa s. K depends on the type of gas–liquid interface, and it has been proposed that $K = 9.9 \times 10^{-3}$ for rigid interfaces and $K = 2.3 \times 10^{-3}$ for mobile interfaces.[51] A is then estimated to be 1.2 cm s$^{-1/2}$ for rigid interfaces and 0.6 cm s$^{-1/2}$ for mobile interfaces. This simple comparison suggests that the gas–liquid interface of the SDS or TX-100 aqueous solution in this study would be treated as a mobile interface.[46,51]

In two-dimensional water imbibition under microgravity, A has been reported to be 0.01–0.02 cm s$^{-1/2}$.[48] This value is one order of magnitude smaller than our values. The imbibition front radially spread in that study, whereas it proceeded along the x direction in this work. In addition, because of the difference in the thicknesses of the observed foams, the number ratio of exterior channels to total channels would be larger in this study compared with that in ref. 48. Faster flow velocity in the exterior channels has been reported,[23] and this would contribute to a larger value in A in our work. These factors would cause a different value of A.

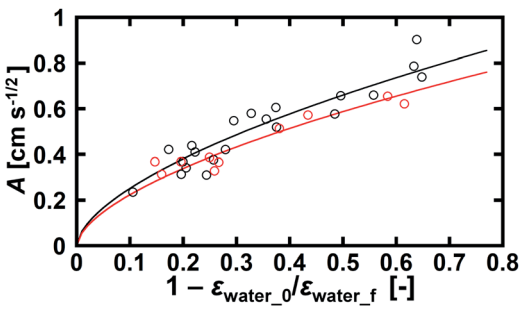

Fig. 8 Correlation between A and $(1 - \varepsilon_{water\_0}/\varepsilon_{water\_f})$. Black and red represent the data of SDS and TX-100, respectively. The power law fits to the data are shown as solid lines with $A = (1 - \varepsilon_{water\_0}/\varepsilon_{water\_f})^{0.6}$ for SDS (black) and $A = 0.89(1 - \varepsilon_{water\_0}/\varepsilon_{water\_f})^{0.6}$ for TX-100 (red).

4.2 Scaling formula for water imbibition

The kinetic constant A describes the initial rate of increase in the imbibition length, but we were not able to describe the later imbibition rate using A. In this section, we derive a dimensionless equation that describes the change of the imbibition length with time over the entire period.

We assumed a constant value of A in eqn (1). However, as clearly shown in Fig. 6, A decreased as water imbibition progressed. We define A_n for A at time t_n. We then rewrite eqn (1) using a recurrence formula as

$$x(t_{n+1}) - x(t_n) = A_n\left(\sqrt{t_{n+1}} - \sqrt{t_n}\right) \quad (2)$$

where $t_{n+1} = t_n + \Delta t$ with Δt being a small time interval. From summation of the right-hand side of eqn (2) from 1 to n, we obtain

$$x(t_{n+1}) - x(t_1) = \sum_{i=1}^{n} A_i\left(\sqrt{t_{i+1}} - \sqrt{t_i}\right) \quad (3)$$

The kinetic constant A_n varies with time because the volume fraction of water in the foam increases during imbibition. We assume that the volume fraction of water in the foam is ε_{water_f} after the tip of water imbibition has passed and the water volume fraction in the rest part of the foam is ε_{water_0}. This assumption is schematically illustrated in Fig. 9. The average water volume fraction in the foam ε_{av} is then

$$\varepsilon_{av} = \varepsilon_{water\_0} + \left(\varepsilon_{water\_f} - \varepsilon_{water\_0}\right)\frac{x(t_n) - x(t_1)}{L_0 - x(t_1)} \quad (4)$$

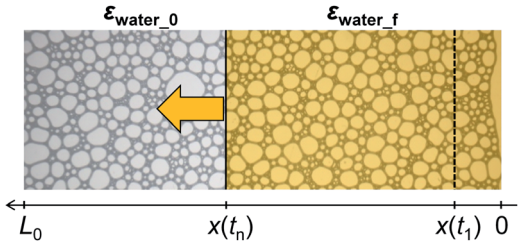

Fig. 9 Schematic illustration of the assumptions for the imbibition length and water volume fraction in the proposed model.

where L_0 is the initial length of the foam before water imbibition. We note that there is a distribution of water volume fractions during imbibition (Fig. 5). Thus, ε_{av} in eqn (4) is used as a representative value for ε_{water}. According to the correlation $A = (1 - \varepsilon_{water\_0}/\varepsilon_{water\_f})^{0.6}$ for the SDS samples in Fig. 8, we introduce the following relation between A_n and ε_{av}:

$$A_n = (1 - \varepsilon_{av}/\varepsilon_{water\_f})^{0.6} \quad (5)$$

We are able to simulate the change of the imbibition length with time using eqn (3)–(5).

We further developed these expressions by introducing the dimensionless length and time. We define the dimensionless length as $\eta_n = (x(t_n) - x(t_1))/(L_0 - x(t_1))$ and the dimensionless time as $\varphi_n = t_n/\tau_{SDS}$, where τ_{SDS} is the characteristic time scale for water imbibition in the SDS samples, which is defined as ${\tau_{SDS}}^{-0.5} = (1 - \varepsilon_{water\_0}/\varepsilon_{water\_f})^{0.6}(L_0 - x(t_1))^{-1}$. For the TX-100 samples, A_n is $0.89(1 - \varepsilon_{av}/\varepsilon_{water\_f})^{0.6}$, which is roughly described as $(\gamma_{TX\text{-}100}/\gamma_{SDS})(1 - \varepsilon_{av}/\varepsilon_{water\_f})^{0.6}$ as discussed in the Section 4.1. In this relation, γ is interfacial energy between water and air, and the subscript denotes surfactants dissolved in water. Then we obtain the ratio of the characteristic times as $\tau_{TX\text{-}100}/\tau_{SDS} = (\gamma_{SDS}/\gamma_{TX\text{-}100})^2$. By substituting these values into eqn (3) and using the relation that $\eta_1 = 0$ from the definition of η_n, we finally obtained the following relation:

$$\eta_{n+1} = \sum_{i}^{n} (1 - \eta_i)^{0.6}\left(\sqrt{\varphi_{i+1}} - \sqrt{\varphi_i}\right) \quad (6)$$

Derivation of eqn (6), τ_{SDS} and $\tau_{TX\text{-}100}$ is given in the Appendix. We scaled all data for SDS and for TX-100 to η_n and φ_n, and they are plotted in Fig. 10. For comparison, the same data before scaling are shown in the inserts of Fig. 10. We found that there was good agreement between the experimental data and the curve simulated using eqn (6). We concluded that eqn (3)–(5) and the dimensionless form of eqn (6) reasonably quantitatively describe water imbibition.

One important point is that we did not use microscopic parameters, such as r_{curv} and L_{nn}, in the above equations. They have been used as essential factors in theoretical approaches of the flow in foams. However, our results clearly showed that we did not need to evaluate these parameters for water imbibition. From eqn (4), the dimensionless water volume fraction of $(\varepsilon_{av} - \varepsilon_{water\_0})/(\varepsilon_{water\_f} - \varepsilon_{water\_0})$ is equal to η_n. Thus, another

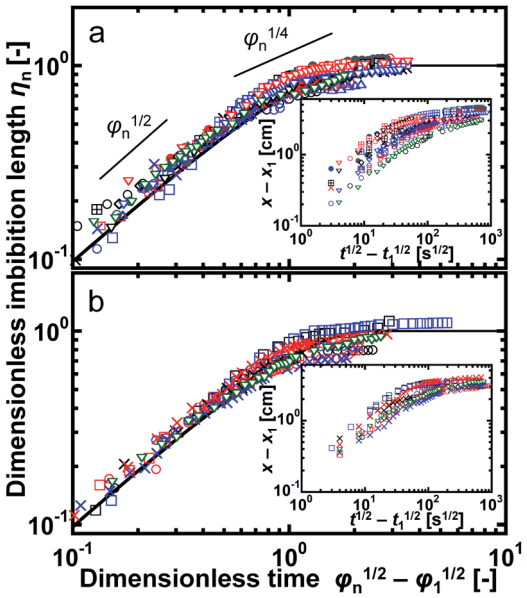

Fig. 10 Plots of the dimensionless imbibition length η_n and time φ_n for foams of (a) SDS and (b) TX-100. The different symbols represent the data for different samples. The solid lines in (a) and (b) were obtained with eqn (6), and they show good agreement with the experimental data. The inserts show the same data but not in a dimensionless form, in which x and x_1 correspond to $x(t)$ and $x(t_1)$ in the main text. The two short lines in (a) show the corresponding slopes for η_n in proportion to ${\varphi_n}^{1/2}$ and ${\varphi_n}^{1/4}$.

interpretation of Fig. 10 is time evolution of the average water volume fraction in foams. $(\varepsilon_{av} - \varepsilon_{water\_0})/(\varepsilon_{water\_f} - \varepsilon_{water\_0}) \approx 0.7$ for $\varphi_n - \varphi_1 \approx 1$, around which the rate of water imbibition gradually decreased. In most cases, $\varphi_1 \ll 1$, and thus $t \approx \tau$ is the characteristic time for the beginning of the decrease in the rate of water imbibition.

In the initial stage of imbibition, η_n was proportional to ${\varphi_n}^{1/2}$ (Fig. 10). This feature is observed in three different experimental systems: water imbibition under microgravity,[45,46] oil imbibition under gravity,[42] and horizontal oil imbibition in aqueous foams in a Hele-Shaw cell.[52] In the first case, the gravity effect is negligible and water imbibition is induced by the capillary pressure in the dry foam. Mensire *et al.*[42] observed 3D oil imbibition in a dry foam under gravity. They proposed a physical model that considers a balance between gravity and the vertical capillary pressure, Darcy's law, and conservation of mass in the foam, with which they succeeded in describing the $t^{1/2}$ dependence of the tip position of imbibition.[42] Kusaka *et al.*[52] reported horizontal oil imbibition, and they explained the $t^{1/2}$ dependence of the tip position using a simple form of Darcy's law. Our data agrees with these results, and we conclude that the $t^{1/2}$ dependence of the imbibition tip is a general feature independent of the imbibition direction (horizontal or vertical) and type of liquid (water or oil).

In the late stage of imbibition, the rate of imbibition gradually decreased (Fig. 10). Mensire *et al.*[42] reported that the time dependence of the tip position was $t^{1/4}$ in 3D imbibition, while a theoretical approach predicted $t^{1/3}$.[33] The differences in the boundary conditions between theory and experiment have been

suggested to be a reason for the discrepancy.[42] Horizontal oil imbibition shows $t^{1/3}$ dependence of the imbibition front.[52] Thus, the time dependence is still under debate. Our data showed approximate agreement with the slope of ${\varphi_n}^{1/4}$ around $\varphi_n \approx 1$ (Fig. 10), but the slope of the data clearly decreased for further imbibition. Thus, our data did not show any constant time dependence of the tip position in the late stage of imbibition. One reason is the small ratio of the imbibition length to the total length of the foam. In the 3D imbibition study,[42] the reported tip position was about 10 mm in a foam with a height of 5 cm. For the horizontal oil imbibition study,[52] an imbibition length of 10 mm was observed for a circular foam with a diameter of 55 mm, which was estimated from the experimental conditions. The ratio was approximately 0.2 in both cases. In the above studies, the liquid imbibed from the edge of the foam, but the observed tip position was away from the other edge, suggesting that the end of the foam could be assumed to be an infinite boundary for imbibition. In contrast, in this study, imbibition reached very close to the end of the foams and the infinite boundary condition was not a suitable assumption. Imbibition occurs in a foam, and imbibition will stop when the front reaches the end of the foam. Therefore, the rate of imbibition decreased when η_n was close to unity, and this effect is expressed as $(1 - \eta_n)^{0.6}$ in eqn (6).

In vertical capillary rise experiments, there is a maximum height at which the capillary pressure balances with the gravity.[53] However in horizontal imbibition, the gravity is negligible in general[54] and there is no clear prediction on the maximum length for the imbibition. But our results clearly show that there is a termination in horizontal imbibition in foams when the foams are filled with imbibed liquid. Another important point is that we used an expression of $t^{1/2}$ dependence for scaling. In most previous papers on imbibition or capillary rise experiments, imbibition kinetics is considered separately with a different scaling law. Different imbibition regimes are expressed by different power laws of time, such as $t^{1/2}$, $t^{1/3}$ or $t^{1/4}$ in these papers.[33,42,52] We used a combination of $t^{1/2}$ dependence and a valuable of A, which was a function of the volume fraction of water in foams during imbibition. This is not a general approach. However we have succeeded in describing water imbibition over the entire period of imbibition using a single formula of eqn (6) as shown in Fig. 10. Gradual decrease in the rate of imbibition was not described by the power law of $t^{1/2}$, but it was described by a decrease in A in our model. We conclude that the volume fraction of water during imbibition is a key to describe imbibition.

We note that coalescence or coarsening of bubbles occurred during imbibition but it was infrequent. In addition, the timescale for coarsening was about 10^3 s in this study. Water imbibition was much faster than this time scale and we consider that bubbles in this work was stable during observation. We also note that coarsening and coalescence generally occurs when bubbles are in close contact. However, in the final stage of water imbibition, the water volume fraction in foam is large and bubbles are separated by thick water layer as in Fig. 4c. Thus even if coalescence or coarsening of bubbles would affect water imbibition in this study, it would be observed in the initial stage of imbibition, in which foam is still dry.

In flow of an oil in a single aqueous Plateau border, the imbibition dynamics of the oil obey the $t^{2/3}$ law in the initial stage of imbibition, during which there is oil flow from the soap film to the Plateau border.[10] It then changes to the $t^{1/3}$ law after all of the oil has entered the Plateau border.[10] These features were not observed in our study. This clearly shows that imbibition in foams is not simple summation of the flows in the individual Plateau borders. Different flow velocities in the exterior and interior channels,[23] complicated flow in the nodes,[23,25] and connection of many Plateau borders through nodes would cause different imbibition features from the liquid flow in a single Plateau border.

We found that the average liquid volume fraction of water is the key factor to describe the kinetics of the imbibition front. This is important to predict the imbibition front in a simple way and could be used for liquid transport on two-dimensional cell sheets. However, several open questions remain. The followings are two examples. First, what is the physical background for why A is proportional to $(1 - \varepsilon_{\mathrm{water\_0}}/\varepsilon_{\mathrm{water\_f}})^{0.6}$? Second, what is the link between the microscopic parameters, such as r_{curv} and L_{nn}, and the macroscopically determined $\varepsilon_{\mathrm{water}}$, especially for a system of a polydisperse foam? Theoretical approaches are necessary to answer these questions. We believe that further investigation of these questions will reveal the hidden physical background of liquid imbibition in foams.

5. Conclusions

Our main findings are the following points.

- The progression in the tip position of water imbibition in polydisperse foams is proportional to the square root of time during the initial stage of imbibition, but the kinetic (proportional) constant A gradually decreases during further water imbibition.
- The kinetic constant A does not show any clear correlation to the radius of curvature and channel length in the polydisperse foams before imbibition. Conversely, the volume fraction of water closely relates to the kinetic constant A.
- All data is well summarized by the dimensionless recurrence formula, which is obtained from the $t^{1/2}$ dependence of the tip position and the correlation of A with the water volume fraction during imbibition. This suggests that the formula can be used as a general scaling law for water imbibition.

We consider that these findings in this work provide a new framework for theoretical approaches in understanding the scaling law for the kinetics in water imbibition in foams.

6. Appendix

From eqn (4), $\varepsilon_{\mathrm{av}} = \varepsilon_{\mathrm{water\_0}} + (\varepsilon_{\mathrm{water\_f}} - \varepsilon_{\mathrm{water\_0}})\eta_n$ and we obtain a different expression for A_n:

$$A_n = (1 - \varepsilon_{\mathrm{water\_0}}/\varepsilon_{\mathrm{water\_f}})^{0.6}(1 - \eta_n)^{0.6} \tag{A-1}$$

The imbibition length and time are expressed as $x(t_n) - x(t_1) = (L_0 - x(t_1))\eta_n$ and $t_n = \varphi_{\mathrm{n}}\tau_{\mathrm{SDS}}$. By substituting these expressions and eqn (A-1) into eqn (3), we obtain

$$\eta_{n+1} = \left(1 - \frac{\varepsilon_{\mathrm{water\_0}}}{\varepsilon_{\mathrm{water\_f}}}\right)^{0.6} \frac{\sqrt{\tau_{\mathrm{SDS}}}}{L_0 - x(t_1)} \sum_i^n (1 - \eta_i)^{0.6}\left(\sqrt{\varphi_{i+1}} - \sqrt{\varphi_i}\right) \tag{A-2}$$

Thus, ${\tau_{SDS}}^{-0.5} = (1 - \varepsilon_{water\_0}/\varepsilon_{water\_f})^{0.6}/(L_0 - x(t_1))$ is defined as the characteristic time scale for water imbibition in the SDS samples, with which the final form of the dimensionless formula of eqn (6) is obtained. For TX-100, A_n is approximately defined as $(\gamma_{TX\text{-}100}/\gamma_{SDS})(1 - \varepsilon_{water\_0}/\varepsilon_{water\_f})^{0.6}(1 - \eta_n)^{0.6}$ and this leads $(\tau_{TX\text{-}100}/\tau_{SDS}) = (\gamma_{SDS}/\gamma_{TX\text{-}100})^2$ as in the main text.

Author contributions

K. T. conducted the experiments and data validation, and drafted the first draft of the manuscript. S. I. contributed to the concept and design of the study, funding acquisition, and reviewed and edited the manuscript.

Conflicts of interest

There are no conflicts to declare.

Acknowledgements

We thank Tim Cooper, PhD, from Edanz Group (https://jp.edanz.com/ac) for editing a draft of this manuscript. This work was partially financially supported by JSPS KAKENHI, Grant Number JP21K18843.

References

1 L. Saulnier, W. Drenckhan, P. –E. Larre, C. Anglade, D. Langevin, E. Janiaud and E. Rio, *Colloids Surf., A*, 2015, **473**, 32–39.
2 A. E. Roth, C. D. Jones and D. J. Durian, *Phys. Rev. E*, 2013, **87**, 042304.
3 F. F. Dunne, F. Bolton, D. Weaire and S. Hutzler, *Philosophical Magazine*, 2017, **97**, 1768–1781.
4 V. Carrier and A. Colin, *Langmuir*, 2003, **19**, 4535–4538.
5 D. Georgieva, A. Cagna and D. Langevin, *Soft Matter*, 2009, **5**, 2063–2071.
6 A. Maestro, W. Drenckhan, E. Rio and R. Hohler, *Soft Matter*, 2013, **9**, 2531–2540.
7 R. Hohler, Y. Y. C. San, E. Lorenceau and S. Cohen-Addad, *Langmuir*, 2008, **24**, 418–425.
8 A. Boromand, A. Signoriello, J. Lowensohn, C. S. Orellana, E. R. Weeks, F. Ye, M. D. Shattuch and C. S. O'Hern, *Soft Matter*, 2019, **15**, 5854–5865.
9 F. Zaccagnino and S. Cox, *Soft Matter*, 2020, **16**, 8861–8870.
10 K. Piroird and E. Lorenceau, *Phys. Rev. Lett.*, 2013, **111**, 234503.
11 A. Cohen, N. Fraysse and C. Raufaste, *Phys. Rev. E*, 2015, **91**, 053008.
12 A. Cohen, N. Fraysse, J. Rajchenbach, M. Argentina, Y. Bouret and C. Raufaste, *Phys. Rev. Lett.*, 2014, **112**, 218303.
13 C. Clarke, A. Lazidis, F. Spyropoulos and I. T. Norton, *Soft Matter*, 2019, **15**, 1879–1889.
14 S. A. Koehler, S. Hilgenfeldt, E. R. Weeks and H. A. Stone, *J. Colloid Interface Sci.*, 2004, **276**, 439–449.
15 O. Pitois, C. Fritz and M. Vignes-Adler, *Colloids Surf., A*, 2005, **261**, 109–114.
16 G. Lin, J. Frostad and G. Fuller, *Physical Review Fluids*, 2018, **3**, 114001.
17 A. Ponomarenko, D. Quere and C. Clanet, *J. Fluid Mech.*, 2011, **666**, 146–154.
18 M. J. Kennedy, M. W. Conroy, J. W. Fleming and R. Ananth, *Colloids Surf., A*, 2018, **540**, 158–166.
19 O. Pitois, N. Louvet, E. Lorenceau and F. Rouyer, *J. Colloid Interface Sci.*, 2008, **322**, 675–677.
20 K. Piroird, E. Lorenceau and A. –L. Biance, *Soft Matter*, 2014, **10**, 7061–7067.
21 R. A. Leonard and R. Lemlich, *AIChE J.*, 1965, **11**, 18–25.
22 H. M. Princen, *J. Colloid Interface Sci.*, 1979, **71**, 55–66.
23 S. A. Koehler, S. Hilgenfeldt and H. A. Stone, *J. Colloid Interface Sci.*, 2004, **276**, 420–438.
24 B. Gay, P. Rognon, D. Reinelt and F. Molino, *Eur. Phys. J. E*, 2011, **34**, 2.
25 A. Anazadehsayed, N. Rezaee and J. Naser, *J. Colloid Interface Sci.*, 2017, **504**, 485–491.
26 A. Anazadehsayed, N. Rezaee and J. Naser, *J. Colloid Interface Sci.*, 2018, **511**, 440–446.
27 A. Anazadehsayed, N. Rezaee, J. Naser and A. V. Nguyen, *Adv. Colloid Interface Sci.*, 2018, **256**, 203–229.
28 H. Feng, J. H. B. Sprakel, D. S. Ershov, T. Krebs, M. A. Cohen Stuart and J. van der Gucht, *Soft Matter*, 2013, **9**, 2810–2815.
29 H. Feng, J. Sprakel and J. van der Gucht, *Phys. Rev. E*, 2015, **92**, 023011.
30 K. Hasegawa and S. Inasawa, *Soft Matter*, 2017, **13**, 7026–7033.
31 K. Hasegawa and S. Inasawa, *Soft Matter*, 2020, **16**, 8692–8701.
32 B. Weaire, N. Pittet, S. Hutzler and D. Pardal, *Phys. Rev. Lett.*, 1993, **71**, 2670–2673.
33 S. A. Koehler, H. A. Stone, M. P. Brenner and J. Eggers, *Phys. Rev. E*, 1998, **58**, 2097–2106.
34 S. J. Neethling, H. T. Lee and J. J. Cilliers, *J. Phys.: Condens. Matter*, 2002, **14**, 331–342.
35 A. Saint-Jalmes, *Soft Matter*, 2006, **2**, 836–849.
36 A. Saint-Jalmes, Y. Zhang and D. Langevin, *Eur. Phys. J. E*, 2004, **15**, 53–60.
37 P. M. Kruglyakov, S. I. Karakashev, A. V. Nguyen and N. G. Vilkova, *Curr. Opin. Colloid Interface Sci.*, 2008, **13**, 163–170.
38 E. Lorenceau, N. Louvet, F. Rouyer and P. Pitois, *Eur. Phys. J. E*, 2009, **28**, 293–304.
39 M. Schneider, Z. Zou, D. Langevin and A. Salonen, *Soft Matter*, 2017, **13**, 4132–4141.
40 N. Koursari, P. Johnson, M. Parsa, M. Schneider, A. Trybala and V. M. Starov, *Colloids Surf., A*, 2020, **600**, 124915.
41 B. Haffner, Y. Khidas and O. Pitois, *Soft Matter*, 2014, **10**, 3277–3283.
42 R. Mensire, K. Piroird and E. Lorenceau, *Phys. Rev. E*, 2015, **92**, 053014.
43 R. Mensire, J. T. Ault, E. Lorenceau and H. A. Stone, *Europhys. Lett.*, 2016, **113**, 44002.
44 S. J. Cox and G. Verbist, *Microgravity Sci. Technol.*, 2003, **XIV/4**, 45–52.

45 H. Caps, H. Decauwer, M. –L. Chevalier, G. Soyez, M. Ausloos and N. Vandewalle, *Eur. Phys. J. B*, 2003, **33**, 115–119.
46 H. Caps, S. J. Cox, H. Decauwer, D. Weaire and N. Vandewalle, *Colloids Surf., A*, 2005, **261**, 131–134.
47 A. Saint-Jalmes, S. J. Cox, S. Marze, M. Safouane, D. Langevin and D. Weaire, *Microgravity Sci. Technol.*, 2006, **XVIII-3/4**, 108–111.
48 A. Saint-Jalmes, S. Marze, H. Ritacco, D. Langevin, S. Bail, J. Dubail, L. Guingot, G. Roux, P. Sung and L. Tosini, *Phys. Rev. Lett.*, 2007, **98**, 058303.
49 D. Langevin and M. Vignes-Adler, *Eur. Phys. J. E*, 2014, **37**, 16.
50 H. Caps, N. Vandewalle, A. Saint-Jalmes, L. Saulnier, P. Yazhgur, E. Rio, A. Salonen and D. Langevin, *Colloids Surf., A*, 2014, **457**, 392–396.
51 S. J. Cox, D. Waire and G. Verbist, *Eur. Phys. J. B*, 2004, **40**, 119–121.
52 A. Kusaka, J. Sonoda, H. Tajima and T. Sakai, *J. Phys. Chem. B*, 2018, **122**, 9786–9791.
53 D. Quere, *Europhys. Lett.*, 1997, **39**, 533–538.
54 L. Joly, *J. Chem. Phys.*, 2011, **135**, 214705.